Supplementary Information

Cyanosol-Enabled Ultrafine Alloy Nanocrystals on Graphene as Hybridization Matrix for Long-Life and High-Rate Silicon Anodes

Junwen Zhu[a,§], Xiaoyun Li[a,§], Jingyi Chen[a], Cen Wang,[b] Zhe Li,[b] Xin Cao[a,*], Yiming Zhou[a], Yawen Tang[a] and Ping Wu[a,*]

[a]Jiangsu Key Laboratory of New Power Batteries, Jiangsu Collaborative Innovation Center of Biomedical Functional Materials, School of Chemistry and Materials Science, Nanjing Normal University, Nanjing 210023, PR China.

[b]Berzelius (Nanjing) Co., Ltd., Nanjing, 210012, PR China.

§ J. Zhu and X. Li contributed equally to this work.

E-mail: zjuwuping@njnu.edu.cn (P. Wu), xincao@njnu.edu.cn (X. Cao).

EXPERIMENTAL SECTION

Synthesis of the Si/FeCo/G nanohybrid. In a typical synthesis, solutions of 0.01 M $FeCl_3$ and 0.01 M $K_3Co(CN)_6$ were mixed in equal volumes and dialyzed to form Fe-Co cyanosol. Next, 5 mg of GO powder (DX-GO-33, Shenzhen DX Time Technology Co., Ltd.), with a lateral size of 1-20 μm, was dispersed in 20 mL of deionized (DI) water by ultrasonication. Then, 80 mg polyvinylpyrrolidone (PVP) was added, and the as-prepared PVP-encapsulated GO solution (4.2 mL) was mixed with 16.8 mL of KCl (0.625 M), which was followed by the addition of 0.1 mL of poly (diallyldimethylammonium chloride) (PDDA) (20 wt%) solution. After ultrasonication and washing with DI water, the mixture was dispersed in an additional 4 mL of DI water to form a positively charged GO suspension. Then, 5 mL of Fe-Co cyanosol was added to 15 mL of the positively charged GO solution, and the mixture was ultrasonicated for 2 h. Next, 30 mg of silicon powder (average size of ~50 nm, Alfa Aesar) was added to the mixture to form Si/Fe-Co/GO nanohybrid. The obtained Si/Fe-Co/GO nanohybrid was pyrolyzed at 500 °C for 3 h under N_2 flow to obtain Si/FeCo/G nanohybrid. For comparison, Si/G nanohybrid has also been prepared by pyrolyzing Si/GO nanohybrid instead of Si/Fe-Co/GO nanohybrid by keeping the other conditions unchanged.

Characterization. Scanning electron microscope (SEM, JSM-5610LV), transmission electron microscope (TEM, Hitachi H-7650), and high-tesolution TEM (HRTEM, JEOL JEM-2100F, 200 kV) equipped with an energy-dispersive X-ray spectrometer (EDS, Thermo Fisher Scientific) were employed to characterize the morphologies and microstructures of the samples. The crystalline phases and crystallinity were identified by X-ray Powder Diffraction (XRD, Rigaku D/max 2500/PC). Fourier transform infrared (FTIR) spectra was conducted on a Bruker Tensor 27 spectrometer. Nitrogen adsorption/desorption tests were performed using a Micromeritics ASAP 2460 analyzer, employing both Brunauer-Emmett-Teller (BET) and Barrett-Joyner-Halenda (BJH)

methods for measuring surface area, pore volume and size. Thermogravimetric analysis (TGA) was performed using a thermal analyzer (NETZSCH STA) at a heating rate of 10 °C min^{-1} under an air atmosphere.

Electrochemical Measurements. The working electrodes were prepared using a slurry method, where the synthesized materials were combined with sodium carboxymethyl-cellulose (CMC) and carbon black in a weight ratio of 7:1.5:1.5 in deionized water. This mixture was then spread over copper foil current collectors and dried under vacuum at 90 °C for 12 hours. The lithium storage performance of the products was tested using CR-2025 coin cells which were assembled in an Ar-filled glove box (Innovative Technology, IL-2 GB) using lithium metal foil as the counter electrode. The electrolyte consisted of 1 M $LiPF_6$ in ethylene carbonate (EC)/dimethyl carbonate (DMC) (1:1 in volume), containing 5 vol% fluoroethylene carbonate (FEC). Galvanostatic discharge/charge measurements were performed using a LANHE battery test system (CT2001A) across a 0.01-1.2 V voltage window, starting at 0.1 A g^{-1} for the first cycle and increasing to 0.5-10 A g^{-1} in subsequent cycles. Cyclic voltammetry (CV) tests (0.1-1 mV s^{-1}) and electrochemical impedance (EIS, from 100 kHz to 10 mHz) were performed using a CHI 660E electrochemical station. The $LiCoO_2$ cathode and the Si/FeCo/G anode were used to assemble a full coin cell using the same electrolyte and separator for half cells. The specific capacity ratio of anode and cathode was ≈1.2:1.

Fig. S1 Photograph of the Fe-Co cyanosol and its Tyndall effect.

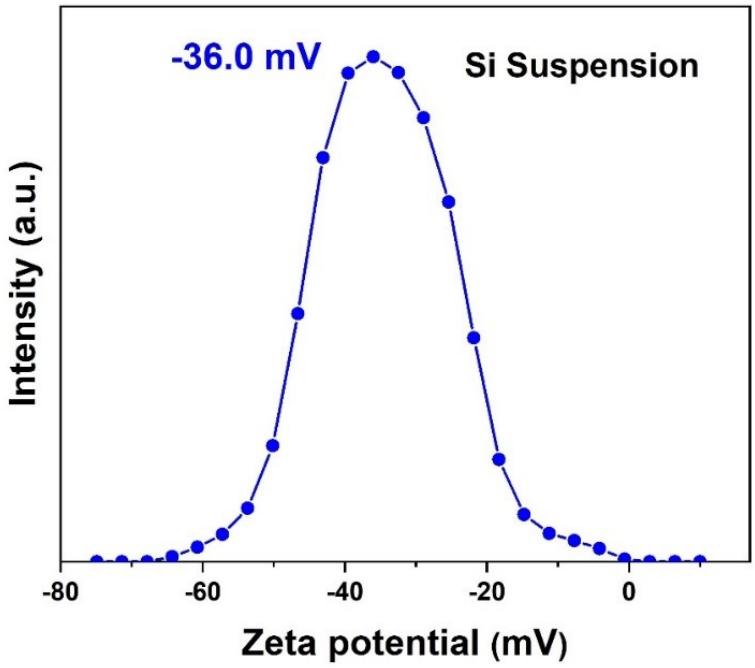

Fig. S2 The zeta potential of the Si suspension.

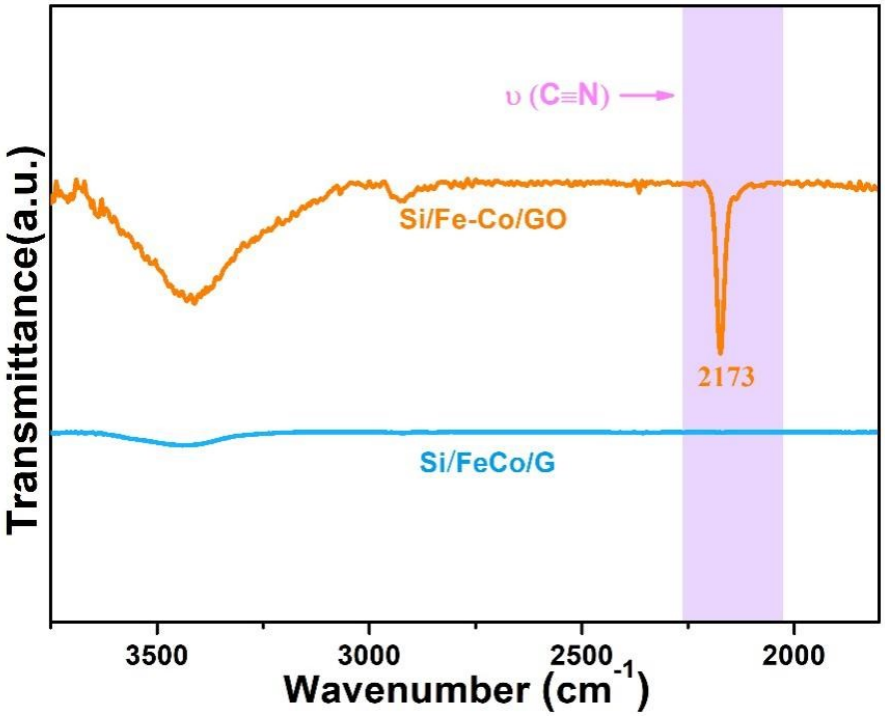

Fig. S3 FTIR spectra of Si/FeCo/G nanohybrid compared with Si/Fe-Co/GO nanohybrid.

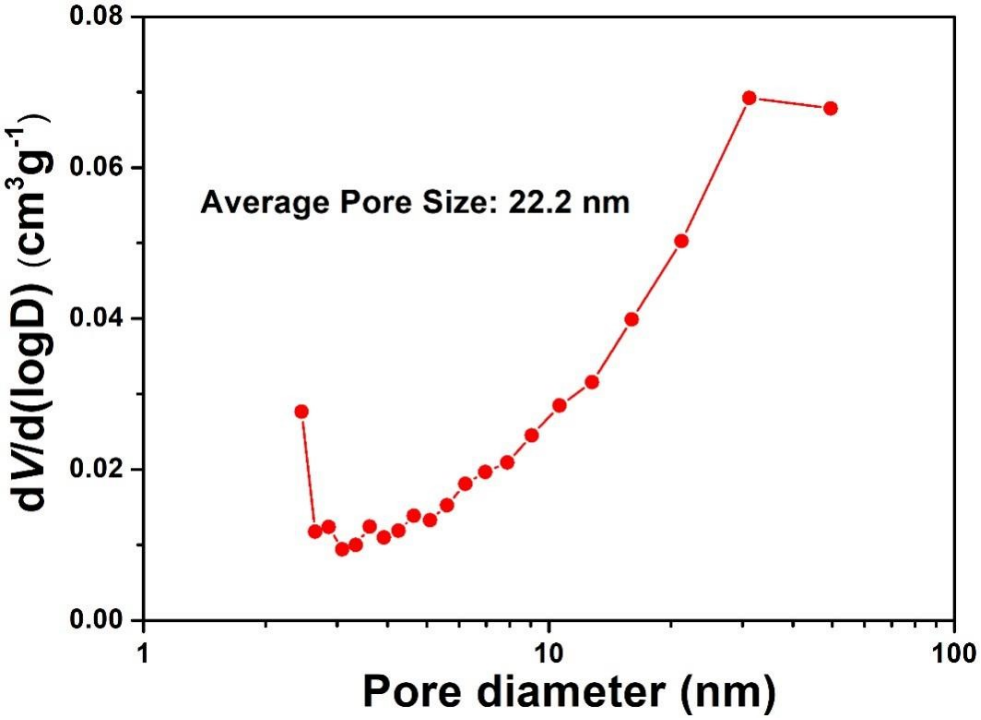

Fig. S4 Pore size distribution of the Si/FeCo/G nanohybrid.

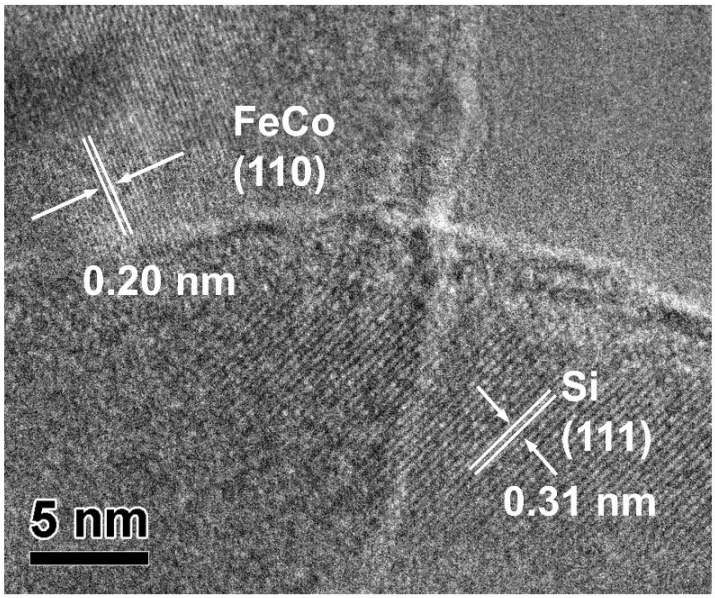

Fig. S5 HRTEM image of the Si/FeCo/G nanohybrid with lattice fringes of Si and FeCo components.

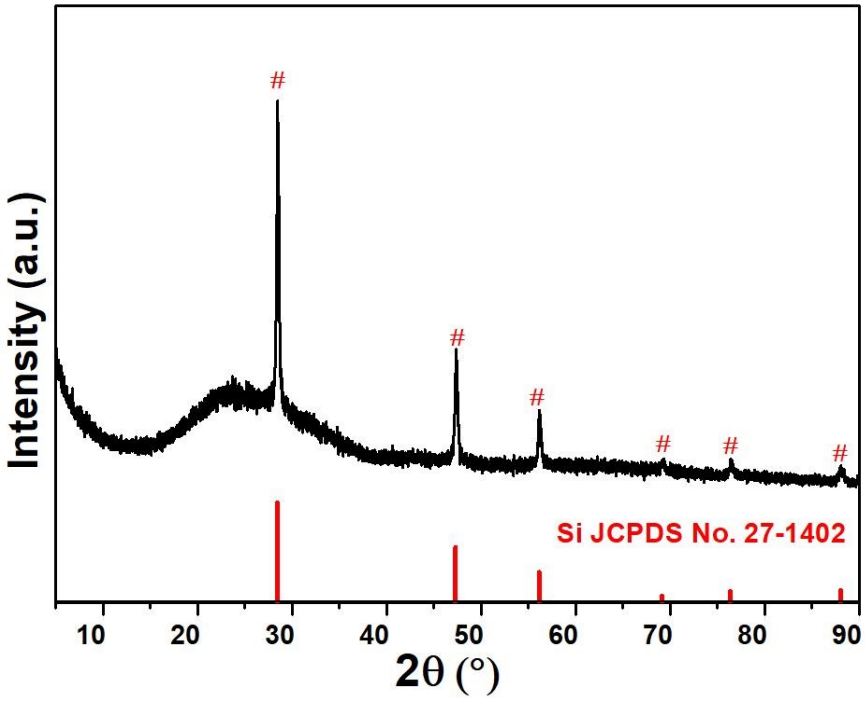

Fig. S6 XRD pattern of Si/G nanohybrid.

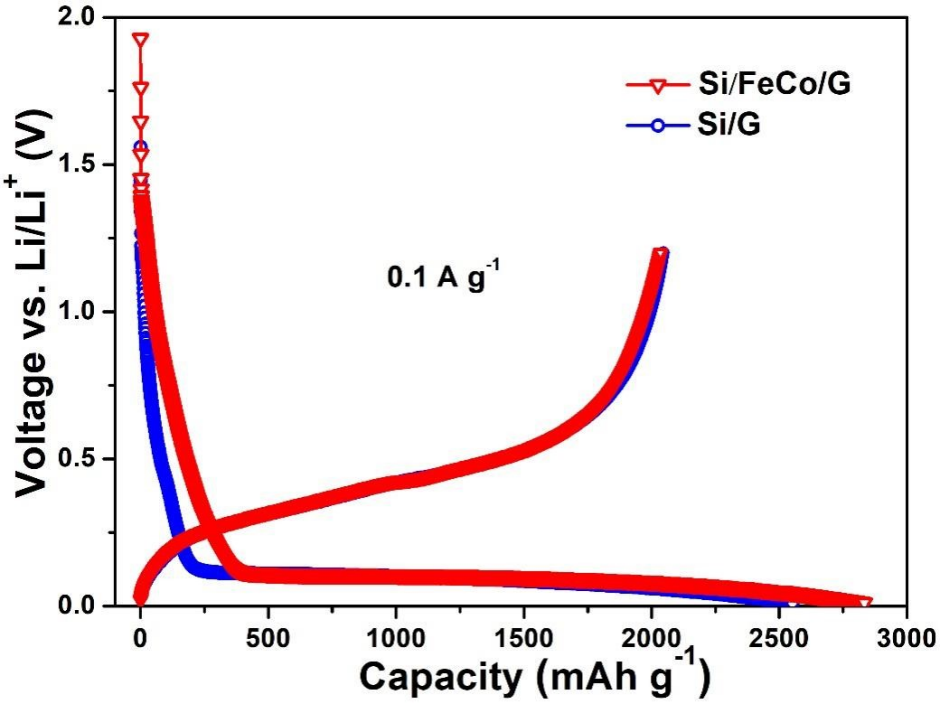

Fig. S7 Initial discharge and charge curves of Si/FeCo/G anode compared with Si/G anode.

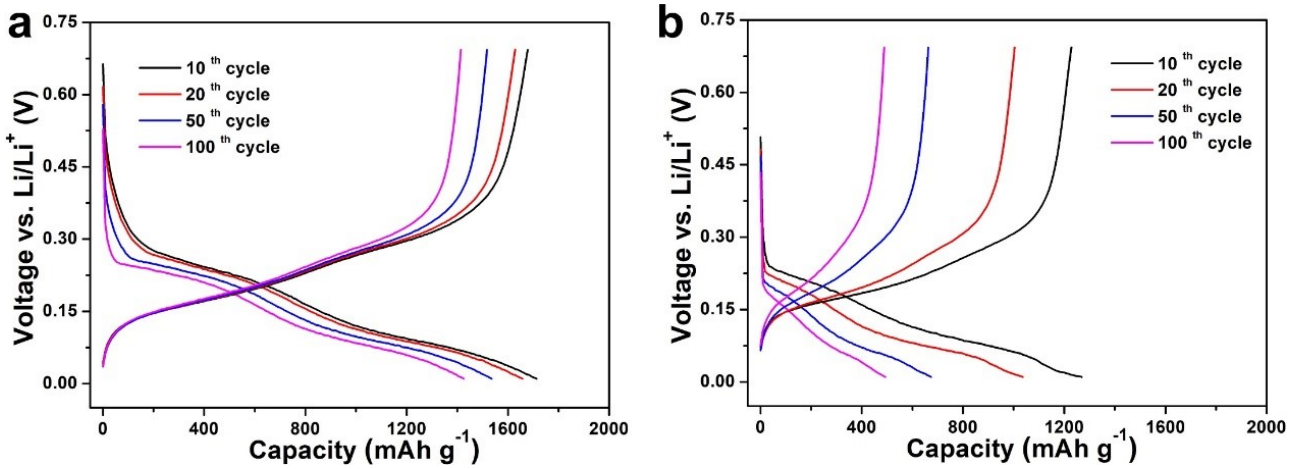

Fig. S8 Discharge and charge curves in 10^{th} , 20^{th} , 50^{th} , 100^{th} cycles of (a) Si/FeCo/G anode and (b) Si/G anode.

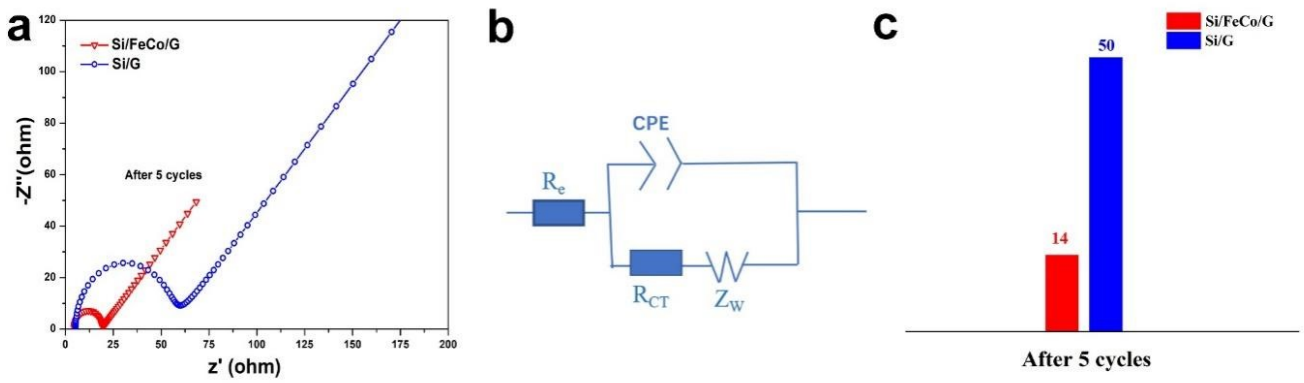

Fig. S9 (a) Nyquist plots from impedance tests of the Si/FeCo/G and Si/G anodes. (b) The equivalent circuit model for the fitting of impedance plots. (c)The calculated R_{ct} of Si/FeCo/G anode compared with Si/G anode.

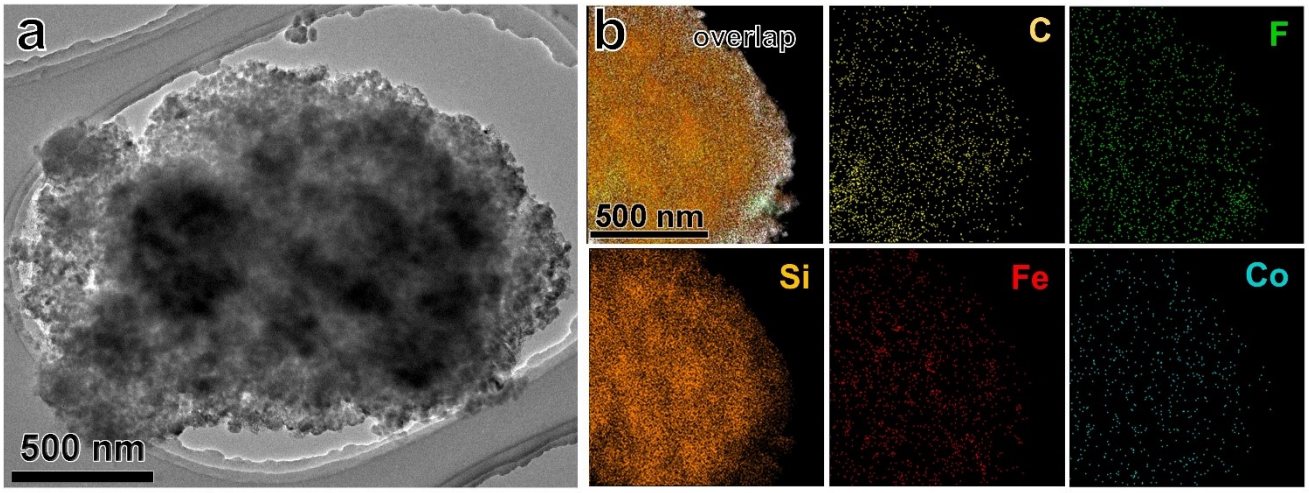

Fig. S10 (a) TEM image and (b) EDS elemental mappings of Si/FeCo/G anode in a fully delithiated state (1.2 V vs Li^+/Li) after cycling.

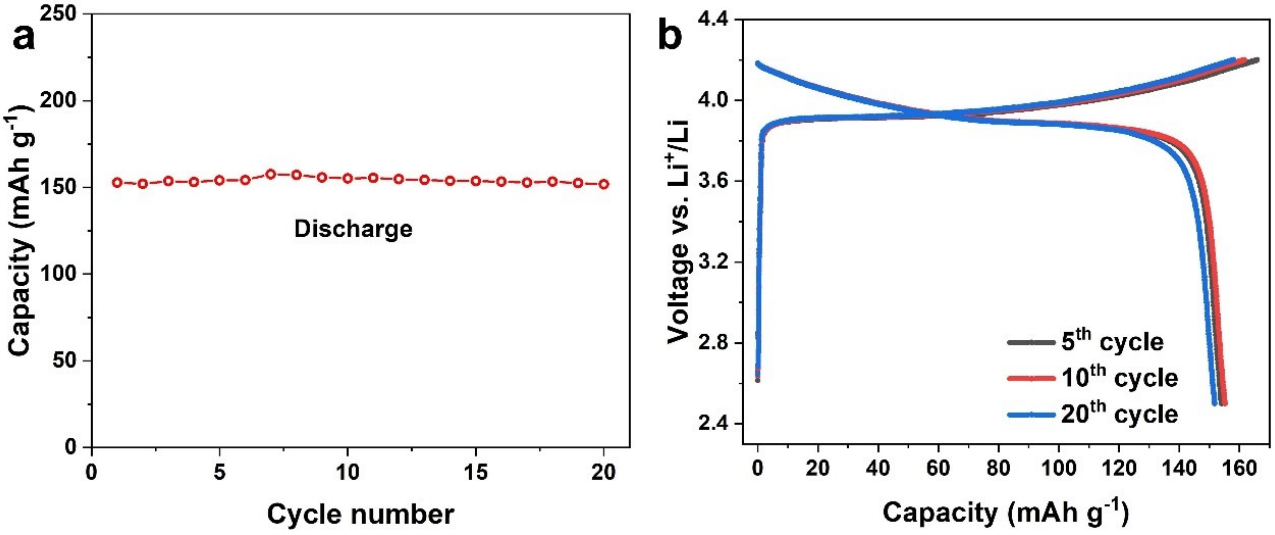

Fig. S11 (a) Cycling performance and (b) discharge and charge curves in 5^{th} , 10^{th} , 20^{th} cycles of $LiCoO_2$ in half cells.

Table S1 Comparison of the lithium storage performance between the Si/FeCo/G anode and previous Si-M-C ternary anodes.

Anode materials	Cycling stability (mAh g^{-1})	Rate capability (mAh g^{-1})	Ref
Si/FeCo/G nanohybrid	**1426 at 0.5 A g^{-1} (100 cycles)**	**1806 at 0.5 A g^{-1} 1118 at 10 A g^{-1}**	**This work**
$FeSi_2$/Si@C composite	1085 at 0.1 A g^{-1} (100 cycles)	1010 at 0.1 A g^{-1} ~710 at 1 A g^{-1}	1
Si–Cu–C/RGO/CNT composite	~1260 at 2 A g^{-1} (100 cycles)	1866.7 at 0.5 A g^{-1} 821.4 at 10 A g^{-1}	2
Si/FeCo@G framework	974 at 0.5 A g^{-1} (100 cycles)	1523 at 0.5 A g^{-1} 417 at 10 A g^{-1}	3
Si–Sn–DHCNF	~ 569 at 0.1 A g^{-1} (100 cycles)	~858.3 at 0.5 A g^{-1} ~ 746.3 at 10 A g^{-1}	4
Si-Sn@G gel framework	983 at 0.5 A g^{-1} (100 cycles)	1222 at 0.5 A g^{-1} 514 at 10 A g^{-1}	5
Si/Ag/C nanohybrids	699 at 0.2 A g^{-1} (100 cycles)	988 at 0.5 A g^{-1} 299 at 5 A g^{-1}	6
Si-SiC/G framework	1060 at 0.5 A g^{-1} (100 cycles)	1151 at 0.5 A g^{-1} 441 at 10 A g^{-1}	7
$Si_{20}Co_{10}C_{70}$ composites	610 at 0.05 A g^{-1} (50 cycles)	NA	8
nanoporous Si-Co-C	1837 at 0.5 A g^{-1} (100 cycles)	2237 at 0.5 A g^{-1} 1318 at 10 A g^{-1}	9
Si-$FeSi_2$-G-C composite	~918 at 0.2 A g^{-1} (80 cycles)	~700 at 1.2 A g^{-1} ~550 at 2 A g^{-1}	10
Si/Cu/C composite	1560 at 0.5 A g^{-1} (80 cycles)	1743 at 0.5 A g^{-1} 577 at 10 A g^{-1}	11

References

[1] Y. Chen, J. Qian, Y. Cao, H. Yang, X. Ai, *ACS Appl. Mater. Interfaces*, 4 (2012) 3753-3758.

[2] Y. Jiang, F. Xiang, S. Fan, Z. Sun, *New J. Chem.*, 45 (2021) 21591-21598.

[3] X. Li, C. Xu, T. Xia, C. Wang, Z. Li, Y. Zhou, *J. Alloys Compd.*, 927 (2022) 167085.

[4] B. Lee, H. Yang, K. Lee, S. Han, W. Yu, *Energy Storage Mater.*, 17 (2019) 62-69.

[5] C. Xu, T. Xia, C. Wang, Z. Li, X. Li, Y. Zhou, *J. Power Sources*, 530 (2022) 231290.

[6] S. Yin, D. Zhao, Q. Ji, Y. Xia, S. Xia, X. Wang, M. Wang, J. Ban, Y. Zhang, E. Metwalli, X. Wang, Y. Xiao, X. Zuo, S. Xie, K. Fang, S. Liang, L. Zheng, B. Qiu, Z. Yang, Y. Lin, L. Chen, C. Wang, Z. Liu, J. Zhu, P. Muller-Buschbaum, *ACS Nano*, 12 (2018) 861-875.

[7] C. Xu, T. Xia, X. Li, A. Zhang, Y. Chen, C. Wang, R. Lin, Z. Li, P. Dai, Y. Zhou, P. Wu, Y. Tang, *Surf. Coating Technol.* 420 (2021) 127336.

[8] J. Zhang, Y. Liang, Q. Zhou, Y. Peng, H. Yang, *J. Power Sources*, 290 (2015) 71-79.

[9] Z. Zhan, T. Huang, J. Zhu, X. Cao, Y. Zhou, Y. Tang, P. Wu, *CrystEngComm*, 26 (2024) 639-646.

[10] H. Kwon, A. Park, S. Lee, H. Cho, H. Jung, C. Park, *J. Electrochem. Soc.*, 166 (2019) A2221-A2229.

[11] N. Lin, J. Zhou, J. Zhou, Y. Han, Y. Zhu, Y. Qian, *J. Mater. Chem. A*, 3 (2015) 17544-17548.